crystals

MDPI

Article

The Effects of Annealing Temperatures and Dimethylformamide Doses on Porous TiO_2 Films

Pao-Hsun Huang [1], Cheng-Han Wu [2], Cheng-Kuan Wu [2], Yu-Quan Zhu [1], Jing Liu [1], Kuan-Wei Lee [2,*] and Chien-Jung Huang [3,*]

[1] School of Ocean Information Engineering, Jimei University, Jimei District, Xiamen 361021, China
[2] Department of Electronic Engineering, I-Shou University, Kaohsiung 84001, Taiwan
[3] Department of Applied Physics, National University of Kaohsiung, Kaohsiung University Road, Kaohsiung 81148, Taiwan
* Correspondence: kwlee@isu.edu.tw (K.-W.L.); chien@nuk.edu.tw (C.-J.H.)

Abstract: In this study, we develop a facile and feasible synthetic technique for producing denser porous titanium dioxide (TiO_2) films. The porous TiO_2 films are effectively prepared using a sol–gel process with dimethylformamide (DMF). The TiO_2 solution is synthesized by adjusting DMF doses ranging from 0 to 10 wt%, and the as-grown TiO_2 films are further annealed at different temperatures from 300 to 500 °C. The TiO_2 films exhibit an asymmetry anatase TiO_2 phase as annealing temperatures increase, and a denser structure as DMF doses increase. The optical properties of all samples are studied, and the porous TiO_2 obtained by 7.5 wt% DMF dose demonstrates a remarkable transmittance and reflectance of 51.87% and 27.55%, respectively, in the visible region from 350 to 850 nm when compared to the pure TiO_2 films. The calculated band gap values range from 3.15 to 3.25 eV. Furthermore, the resistivity of 350 °C-annealed porous TiO_2 thin film is determined by the Hall effect, revealing an increase from 4.46 to an of average 4.79 ohm · cm after injecting DMF solvent. These findings have the potential to assist a growing number of optoelectronic applications.

Keywords: titanium dioxide (TiO_2); porous; annealing temperature; dimethylformamide; spin-coating

Citation: Huang, P.-H.; Wu, C.-H.; Wu, C.-K.; Zhu, Y.-Q.; Liu, J.; Lee, K.-W.; Huang, C.-J. The Effects of Annealing Temperatures and Dimethylformamide Doses on Porous TiO_2 Films. *Crystals* **2023**, *13*, 61. https://doi.org/10.3390/cryst13010061

Received: 6 November 2022
Revised: 23 December 2022
Accepted: 25 December 2022
Published: 29 December 2022

1. Introduction

Titanium dioxide (TiO_2) films are one of the most widely utilized metal oxide materials due to their desirable chemical, electrical, and optical properties. Indeed, TiO_2, as a promising wide bandgap semiconductor, demonstrates outstanding light transmission, as well as a super high refractive index and insulating characteristics, making it suitable for use as a protective layer for very large-scale integration and optical device manufacture. Furthermore, TiO_2 is commonly used as a substitute for storing gas in silicon dioxide [1,2] and as a replacement for ultra-thin oxide dielectric in logic elements [3–5] due to its high dielectric constant. Additionally, TiO_2 is also used in a variety of emerging electronics, including solar cells [6–11], perovskite-based solar cells [12,13], anti-reflection coatings [7,8], gas sensors [14,15], electrochromic displays [16,17], planar waveguides [4], and field-effect transistors [3,5]. In 1972, multiphase photocatalysts were proposed by two researchers, Fujishima and Honda, via decomposing water on TiO_2 to generate oxygen and hydrogen gas [18]. Since then, an intriguing phenomena of photocatalytic TiO_2 rapidly emerged in academia and industry, and it has been actively used in a wide range of applications, such as self-cleaning surfaces, water and air purification, anti-fog surfaces, anti-corrosion, and for anti-bacterial purposes. Most studies adopting powdered TiO_2 material, however, have found that dispersion and coating are significant challenges. As a result, extensive research on the preparation of TiO_2 films has been conducted, including atomic layer deposition (ALD) [9,11], chemical vapor deposition (CVD) [19,20], physical vapor deposition (PVD) [14,15], spray, dip, or spin-coating, and the sol–gel technique [5–8]. The utilized TiO_2 solutions critically depend on the application and substrate used. The most popular,

titanium tetrachloride ($TiCl_4$) and titanium alkoxide [20,21], are usually employed in ALD, CVD, and PVD, whereas solutions of sol–gel TiO_2 [17,18] are utilized via spray, dip, and spin-coating. In comparison to the complicated equipment needed in ALD, CVD, and PVD, nanoscale TiO_2 thin films can be obtained by using the popularized sol–gel technique. The sol–gel technique is a cost-effective method and there is good control over the chemical composition of the products due to the low reaction temperature. Furthermore, it is a conventional and industrial method for the synthesis of nanoparticles with different chemical compositions. The basis of the sol–gel technique is also the production of a homogeneous sol from the precursors and its conversion into a gel. The solvent in the gel is then removed from the gel structure, and the remaining gel is dried [22]. The above statements reveal the advantages of convenience, controllability, and repeatability for the sol–gel technique.

Currently, avoiding the aggregation of TiO_2 nanoparticles during the sol–gel preparation process is a key issue. The TiO_2 samples annealed at 750 °C via microwave-assisted hydrothermal reaction consist of larger aggregated particles with diameters of 500–900 nm, and still retain a mesoporous anatase structure, but with a reduced specific surface area [23]. The TiO_2 microspheres synthesized by ultrasonic spray pyrolysis have a crystallite size of 8 nm and a specific surface area of 27 $m^2 \cdot g^{-1}$, and were produced as soft spherical agglomerates of ~0.6 mm [24]. It is found that the appropriate addition of different kinds or amounts of organic solvents suggests the result of homogeneous dispersion of sol–gel TiO_2 [25]. Meanwhile, high temperatures can be used to treat amorphous TiO_2 sol–gel to obtain the porous TiO_2 films with anatase phase [25,26]. The preparation of porous TiO_2 thin films is notably useful for their higher photoactivity than compact films due to the benefit of a higher surface area, despite the limitation of low adhesive strength and poor compactness, both of which are difficult to improve. The dense TiO_2 film can be prepared by heating or annealing the porous characteristic under the proper temperature control, improving the disadvantages of porous TiO_2 film, such as low mechanical strength, low adhesive strength on the substrate, and the lower transmittance. On the other hand, among the solvents that were used, dimethyl sulfoxide (DMSO) was thought to be more useful due to its relatively less dangerous nature [27]. To improve transmittance, DMSO is commonly used as a formulation additive in the preparation of the TiO_2 electron transport layer (ETL) of perovskite solar cells [28]. Furthermore, this study has compared the optical differences in TiO_2 ETL prepared by distilled water and dimethylformamide (DMF), respectively. On the surface of TiO_2 films, before annealing in air gas, another treatment has been found; a mixed solution of titanium (IV) isopropoxide (TTIP), ethanol, distilled water, and HNO_3 was spin-coated with Cs_2CO_3 that had been dissolved in a $CH_3OCH_2CH_2OH$ solution. Acid-treated TiO_2 films, such as HCl and H_2SO_4, are another option for improving dye-sensitized solar cell performance [29] due to a rougher surface and more hydroxyl groups, resulting in increased surface area and enhanced adherence of the dense TiO_2 film with the porous TiO_2 film by Ti-O-Ti bonds formed by a simple heating process of 150 °C for 10 min. Some research has looked into ethylene glycol and formamide, as well as a mixed solution of N-methylformamide and HF, NH_4F, or KF for the application of the TiO_2 film [30].

One of the proper and most commonly used organic solvents is dimethylformamide (DMF), due to its high dielectric constant, the aprotic nature of the solvent, and its low volatility [7]. The DMF is used in organic synthesis, especially a series of metal carbonyl complexes and a few carbonylative reactions. The DMF is an aprotic solvent that can solventize Ti cations. As the reaction proceeded, the DMF molecules would be taken off from these Ti chelates under high temperature and pressure [31]. However, the decomposition of DMF is difficult due to its high boiling point. The requirement of high temperature and strong acids or bases to volatilize results in the production of carbon and oxygen atoms of the carbonyl group (CO) bonds. The carbon and oxygen atoms can exist in the crystal structure with the defect or interstitial state, and the typical CO-containing volatile organic compounds on an anatase TiO_2 (001) surface can also be calculated by density functional theory [32]. This finding contributes to a better understanding of how the possible production reacted with carbon-containing compounds during volatilization. Currently, there are

many organic solvents acting as a reaction medium, and the Suzuki reaction utilizes the in situ generated CO from photocatalytic DMF decomposition as a CO source [33]. The presence of CO is a proof and incentive to examine the true crystal structure of TiO_2 films by decomposing DMF at high annealing temperatures. The most common application of DMF solvent is to enhance the film compactness, which means making the film more compact. Furthermore, increasing the film compactness is also an excellent functional technique for preventing the recombination of electrons and holes in solar cells [9]. Although DMF is used to inhibit the aforementioned drawbacks, only a few reports discuss the effects of concentration or doses on the post-annealing temperatures for TiO_2 film formation [12,13]. Hamid Latif, et al., reported that the deposition of the compact TiO_2 layer without DMF, but both the active $CH_3NH_3PbBr_3$ layer and spiro-OMeTAD as a hole transport layer were prepared in DMF solution [12]. Govindhasamy Murugadoss, et al., also reported that the perovskite $CH_3NH_3PbI_3$ layer was prepared using a PbI_2 solution dissolved in DMF solvent with stirring at 70 °C. However, the increased current density is attributed to the improved crystal structure obviously induced by DMF solvent via annealing.

Furthermore, the effects of carbon and oxygen atoms and the CO bonds on the preparation of the TiO_2 film should be looked into to find out how organic polar solvents interact with the film after the annealing process. In general, thermal treatment, such as substrate heating or post-deposition annealing, is important for TiO_2 thin films to improve their optoelectrical and structural properties. The most important parameters will be the annealing environment with pure oxygen gas or an atmosphere, the difference in oxygen concentration to cause the oxygen supplementation, and a sufficient or insufficient oxygen lattice for repairing the disordered lattice and improving the crystallinity. Several studies indicate that the annealing process effectively increases the film compactness [34], leading to an increase in mobility, but a slight decrease in transmittance, which is crucially determined by the annealing parameters. In order to obtain the best transmittance and compactness, the parameters of annealing temperatures and solvent doses should be traded off.

In this study, several doses of dimethylformamide (DMF) solvent ranging from 0 to 10 wt% are applied to the solution based on Ti metal. The dynamic spin-coating technique is used to prepare porous TiO_2 thin films. After that, the formed porous films are annealed at temperatures ranging from 300 to 500 °C. The effects of DMF solvent doses and annealing temperatures on the porous TiO_2 thin film, as well as a variety of optical, structural, and electrical properties, are investigated. Meanwhile, the porous TiO_2 thin film prepared achieves the goals of higher transmittance than 50% and lower reflectance than 30% at the visible wavelength range of 400–700 nm to increase the light utilization efficiency for optoelectronics, including solar cells and optical sensors.

2. Materials and Methods

In this paper, all required materials were purchased by the commercial channels and encased in a vacuum moisture-proof box. These materials were not purified before solution preparation. As in our previous research [9–11], the fluorine-doped tin oxide-coated glass substrate (FTO glass (2.2 mm), with a sheet resistance of 7 Ω/sq, AimCore Technology, Hsinchu, Taiwan), and dimensions of 2 cm × 2 cm was cleaned by standard operating procedures. To reduce carbon contamination and improve the surface energy, the FTO glass was treated by 10 W oxygen (O_2) plasma for 2 min (Junsun Tech. Co., Ltd., Taipei, Taiwan) before being transferred to the glove box. The detailed preparation parameters for the TiO_2 solution and film growing are summarized in Table 1.

Table 1. The preparation parameters for the TiO_2 solution and its film growth.

Parameter	Value	Units	Note
Deionized water	3	mL	
[2] Nanopowder TiO_2	2	G	Sigma-Aldrich CAS No. 13463-67-7
Triton-100; [1] d_M = 1.06 g·cm^{-3}	100	µL	Sigma-Aldrich purity: [3] CP
Acetylacetone; [1] d_M = 0.973 g·mL^{-1}	100	µL	Sigma-Aldrich purity: [3] GC
DMF solvent	0 to 10 (0, 2.5, 5, 7.5, and 10)	wt%	Sigma-Aldrich purity: [3] AR
Spin speed	3000	rpm	
Spin time	60	s	
Film growing temperature	180	°C	
Annealing temperature	300 to 500 (300, 350, 400, 450, and 500)	°C	

[1] Here, d_M is the density of material. [2] Nanopowder TiO_2 has a 21 nm primary particle size (TEM), and ≥99.5% trace metals basis. [3] Abbreviations are as follows: CP, chemically pure grade; GC, gas chromatography grade; AR, analytical reagent grade.

2.1. TiO_2 Solution and TiO_2 Thin Films

The preparation for the TiO_2 solution and its film growing was carried out in a glove box with low water and O_2 values. As shown in Figure 1, the TiO_2 solution was mixed using the following materials: titanium oxide (Sigma-Aldrich), Triton-100 (Sigma-Aldrich), acetylacetone (Sigma-Aldrich), deionized water, and DMF (Sigma-Aldrich). It was then was stirred at 300 rpm for 24 h. During the preparation of the TiO_2 solution, the DMF concentration was varied from 0 to 10 wt%, corresponding to the dose dripping by 54, 107, 160, and 216 µL, respectively. The TiO_2 solution was spin-coated with dynamic dispersal on the FTO substrates and then heated on a hotplate to dry the TiO_2 thin film. The thickness of the 350 °C-annealed samples as the DMF dose increased were near 780.5, 785.9, 786.4, 794.9, and 786 nm, respectively. After growing the TiO_2 thin film, the film subsequently received an annealing process in a furnace (RH-274, Tender, Taiwan) at 1 atm in air for 30 min. The annealing temperature was varied from 300 to 500 °C to investigate its influence on the film properties. The sample is placed in the tube during the annealing process. The annealing process has been set up in a three-stage mode, as follows: annealing to 70% temperature set within 30 min in the initial stage and maintaining it for 15 min as the second stage, and then annealing to the temperature set in the third stage. After the annealing process, the samples were cooled down to 40% temperature set within 1 h and then until they reached room temperature within 1 h before being taken out.

2.2. Characteristic Measurement

The crystallite structure was obtained by X-ray diffraction (XRD, Ultima IV, Rigaku Corporation, Tokyo, Japan) on a Philips X's Pert diffractometer equipped with CuKα irradiation (λ = 0.15418 nm) and a fixed power source operating at 40 kV and 40 mA. The XRD patterns were collected in the 2θ range of 10° to 60°, with a step size of 0.06°. The optical properties were measured by the UV–Visible spectrophotometer (UV-3900, Hitachi, Tokyo, Japan). The film thickness (d) was determined by using an alpha-step profilometer (D-500, KLA Tencor Milpitas, CA, USA). The band gap (Eg) of the films was determined by using Tauc's plot method with the following equation: $(\alpha h\nu)^{0.5} = Am(h\nu - Eg)$; where Am is the material dependent constant, hν is the incident photon energy, and α is the absorption coefficient which is illustrated as given by the following: $\alpha = (\ln((1 - R)/T))/d$, where the R and T are the optical reflectance and transmittance of films, respectively. The Eg values of the TiO_2 films are evaluated by plotting $(\alpha h\nu)^{0.5}$ versus hν and extrapolating the linear region of the resultant curves to obtain an interception with the hν-axis. The sample was observed by field-emission scanning electron microscopy (FESEM (0.5 to 30 kV), JEOL 6330, Japan) and high-resolution transmission electron microscopy (TEM (200 kV), JEOL

JEM-2100F CS STEM, Japan) to demonstrate the top-view morphologies and the cross-section images, respectively. Energy-dispersive spectroscopy (EDS, Hitachi S-4800, Oxford Instruments, Shenzhen, China) is used to determine the atomic and weight content of carbon, nitrogen, oxygen, and titanium. Before sample cutting, the sample was capped by a carbon deposited by an E-gun system as a protective layer to prevent damage from Ga ions during sample cutting. The Hall effect analyzer (AHM-800B, advanced design technology, Marchannel Co., Ltd., Shanghai, China) was measured at room temperature to acquire the carrier concentration, mobility, and resistivity.

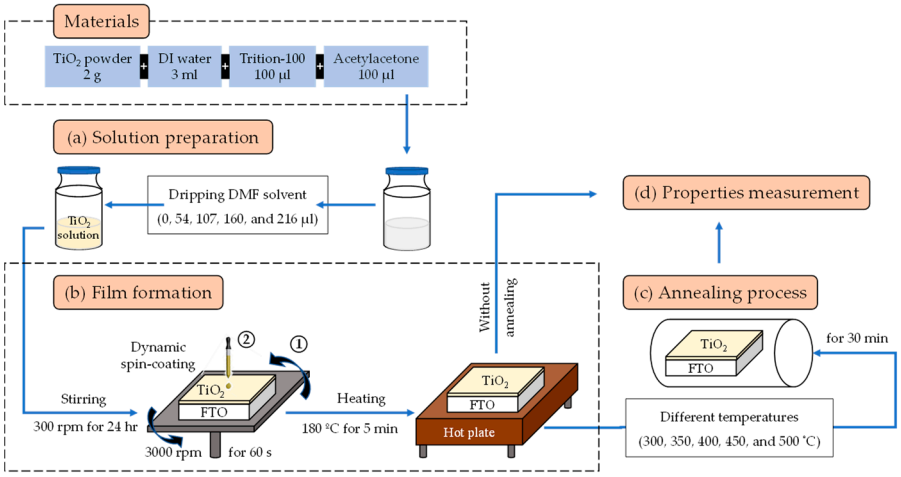

Figure 1. The schematic diagram of TiO_2 preparation, including (**a**) solution preparation injected at different DMF doses from 0 to 10 wt%, (**b**) film formation onto the hotplate, (**c**) annealing process at different temperatures from 300 to 500 °C, and (**d**) properties measurement.

3. Results and Discussion

As shown in Figure 2a, X-ray diffraction (XRD) was used to obtain the diffraction patterns of TiO_2 films at different annealing temperatures from 300 to 500 °C. An obvious (101) peak as a major crystal phase is observed as TiO_2 film is annealed. Based on the diffraction peaks of the TiO_2 films and FTO substrate indexed from the JCPDS card (nos. 71-0652 and 41-1445) [35–37], there is no additional crystal phase growth with the increasing annealing temperatures. Meanwhile, the major peak of (101) observed as the preferred orientation reveals the single-crystal-like structure of TiO_2 films prepared by the 7.5 wt% DMF dose. However, as shown in Figure 2b, a (101) phase at the diffraction angle near 25.32° ± 0.02° observed is asymmetric, and slightly shifts as the increasing annealing temperatures. For example, the peak position shifts to a higher 25.34° and a lower 25.3° as the annealing temperature increases to 350 and 450 °C, respectively. Furthermore, the peak position at 400 and 500 °C shifts to the initial angle, respectively. The reason for the shift of peak position is attributed to the presence of coexisting crystalline phases induced by the phase-transition phenomena between β-TiO_2 and λ-TiO_2 [37]. The non-stoichiometric components of Ti metal may be another reason [38–40]. Some researchers point out that this crystalline phase belongs to the anatase (101), and similar studies for solution engineering via the spin-coating method also reveals the single-crystal-like TiO_2 films [41].

The full width at half maximum (FWHM) value calculated by the Gaussian function in Figure 2c can highlight the intensity variation of the (101) diffraction peak. Notably, as the annealing temperature increases, the highest and lowest FWHM values of 0.178° and 0.305° are obtained at 350 and 500 °C, respectively. The FWHM values at 300, 400, and 450 °C are approximately 0.223°, 0.242°, and 0.223°, respectively. The decrease in FWHM at 350 °C and 450 °C is due to the increase in crystallinity, suggesting a lattice expansion or contraction [42]. Therefore, the grain size (D) and d-spacing from XRD data

are also calculated by using the Scherrer formula and Bragg formula, as in the following Equations (1) and (2), respectively [35–37]:

$$D\ (\beta\cos\theta) = \kappa\lambda, \quad (1)$$

$$2\ đ\ \sin\theta = n\lambda, \quad (2)$$

where, in Equation (1), based on θ, the Bragg angle is the peak position where the κ of 0.9 is the Scherrer constant, and λ is the wavelength of the X-ray sources to estimate the β value by the line broadening at FWHM; in Equation (2), n is the order of diffraction to obtain the d-spacing of *đ*. Furthermore, the micro-strain (ε), and dislocation density (δ) are also calculated, respectively, by the following Equations (3) and (4):

$$\varepsilon = \beta/4tan\theta, \quad (3)$$

$$\delta = \mathrm{m}/\mathrm{D}^2, \quad (4)$$

where the m as a factor is 1. The calculated values are summarized in Table 2. The d-spacing of TiO_2 films varies with the increasing annealing temperatures from 300 to 500 °C, revealing the values of ~3.509, ~3.523, ~3.517, ~3.525 Å, and ~3.525 Å, respectively. It is found that the *đ* at 300 °C is close to the standard value of 3.353 Å, illustrating a lattice expansion of films induced by the chemical reaction [35,36]. In fact, an obvious color difference on the film surface is observed visually after heating on a hotplate. Thus, due to the bad thermal conductivity of the FTO substrate, it can be said that the heating temperature of 180 °C is insufficient to volatilize the DMF solvent (bp = ~153 °C) incompletely, leading to the irregular arrangement and revealing the smaller estimated d-spacing of ~3.51 Å at 300 °C. Increasing the temperature from 300 to 350 °C contributes to atoms being able to acquire more diffusion activation energy to move to energetically favorable lattice sites, causing the lattice expansion and the increase in d-spacing at 350 °C. The decreasing d-spacing at 400 °C evidences the lattice contraction, indicating that the decomposed atoms, such as carbon, nitrogen, and oxygen, are possibly at interstitial sites and able to be released by air annealing. Meanwhile, the role of DMF solvent based on the XRD results not only reveals its assistance in film formation, but also determines the further decomposition as the proper annealing parameters.

Table 2. The XRD results of the 7.5 wt%-injected TiO_2 annealed at different temperatures from 300 to 500 °C.

Annealing Temperatures (°C)	Peak Position (°)	(101) Plane				
		β (°)	*đ* (Å)	D (nm)	$\varepsilon \times 10^{-3}$	$\delta \times 10^{-3}$ (nm^{-2})
300	25.38	0.223	3.5093	36.545	4.3212	0.7488
350	25.32	0.178	3.5229	45.775	3.4633	0.4772
400	25.32	0.242	3.5174	33.672	4.7008	0.8820
450	25.34	0.223	3.5147	36.542	4.3282	0.7489
500	25.34	0.305	3.5147	26.718	5.9197	1.4009

3.1. Effect of Solvent

In Figure 3, the optical properties of TiO_2 films only prepared with different DMF doses from 0 to 10 wt% are demonstrated as the function of wavelength from 350 to 850 nm. The FTO substrate and air were served as the baseline sample to obtain the transmittance and reflectance, respectively. The absorbance was calculated from the transmittance result converted within the instrument. As shown in Figure 3a, with the increasing injection of doses of DMF, there is almost no change in transmittance in the 0 and 2.5 wt% samples. The transmittance increases greatly from 5 to 7.5 wt%, and indicates the highest value at 7.5 wt%. Meanwhile, the reflectance presents the opposite trend to the transmittance in

Figure 3b. The films doped 2.5 wt% DMF have a slight decrease in reflectance compared to the original sample. The reflectance also decreases massively from 5 to 7.5 wt% and demonstrates the lowest value at 7.5 wt%. The reason is possibly attributed to the fact that the chemical interaction between DMF and acetylacetone breaks the bonding of the Ti metal and oxygen [43], further inducing the formation of co-existing crystalline structures in Figure 2. At the same time, the proper addition of DMF solvent inhibits the higher reaction activity [31]. On the other hand, although the hydrolysis product resulting from the DMF solvent also inhibits the TiO_2 crystal growing along the (101) direction, the TiO_2 crystal growth was described as a controlled nucleation–crystallization dissolution process, possibly due to the coordination effect [31]. The variation of transmittance and reflectance (~10%) at short wavelengths is mainly caused by the difference in absorbance, as shown in Figure 3c. Therefore, the haze result in Figure 3d is further calculated by the optical loss equation of $100 - T - R = A$, where T, R, and A are, respectively, transmittance, reflectance, and absorbance; the inserted image is locally enlarged from 500 to 700 nm. As an indicator of the light diffusion, the haze is usually defined as the percentage of light scattering at more than 2.5° from the incident light direction. With the increase in DMF injection, the haze slightly increases and then decreases to the lowest value at 7.5 wt%. As the DMF solvent increases to 10 wt%, the films describe the optical loss of ~2% from the inserted image of Figure 3d due to the optical loss induced by the light scattering. The consequence of light scattering is mainly attributed to the oxygen vacancy defects. The slight absorption of free carriers in oxygen vacancy defects may be another reason, leading to the Eg variation. These results are also similar to a few other studies [44,45].

3.2. Effect of Annealing

The optical properties of 7.5 wt% DMF solvent-induced TiO_2 films prepared at different annealing temperatures from 300 to 500 °C are obtained as shown in Figure 4. The variation of transmittance and reflectance are observed to show opposite trends in Figure 4a,b. With the increasing annealing temperatures, the highest transmittance and the lowest reflectance are demonstrated at 350 °C. As the annealing temperature increases from 350 to 450 °C, the transmittance decreases, and reflectance increases, respectively, and then displays the reverse change at 500 °C. This indicates that the variation between the transmittance is mainly due to the reflectance, which results from the differences in the thickness after annealing. Thus, Figure 4c shows the understandable result of the slight change in absorbance. The reflectance results at 300, 400, and 500 °C show the approximate result in the short wavelength range. However, similar results in the long wavelength range are also observed in the films obtained by 300 and 400 °C, and 350 and 500 °C, respectively, mainly owing to the optical loss induced by light scatting. Therefore, the haze variation, particularly in the long wavelength range, is estimated near 4% in Figure 4d, revealing that the annealing temperatures below 350 °C exhibit no haze change, as with films at temperatures higher than 400 °C.

Figure 5 further illustrates the optical properties of TiO_2 films annealed at 350 °C in which the solution is prepared by different DMF doses from 0 to 10 wt%. Interestingly, as shown in Figure 5a, an obvious increase in transmittance is observed with the increase in DMF injection. When the injected DMF dose is higher than 2.5 wt%, the transmittance of films is closed, with the highest transmittance at 7.5 wt%, and then it decreases at 10 wt%. Compared to the sample without annealing in Figure 3b, the reflectance decreases as the DMF dose increases to 2.5 wt% and it remains almost unchanging at 5 wt% in Figure 5b; however, the TiO_2 films prepared by 7.5 wt% have the lowest reflectance. In general, the compactness of films has an agreement with the increase in DMF doses [46]. The main reason is that the slight DMF injection results in the TiO_2 particle clustering during the crystalline formation [39,40], leading to the increased transmittance and decreased reflectance. However, the excess DMF dose leads to the weakening transmittance and reflectance, probably owing to the abundant bonding of Ti and oxygen. Thus, the absorbance can be

realized in Figure 5c, despite the difference in reflectance, which is due to the haze results in Figure 5d, leading to the closed variation of ~2%.

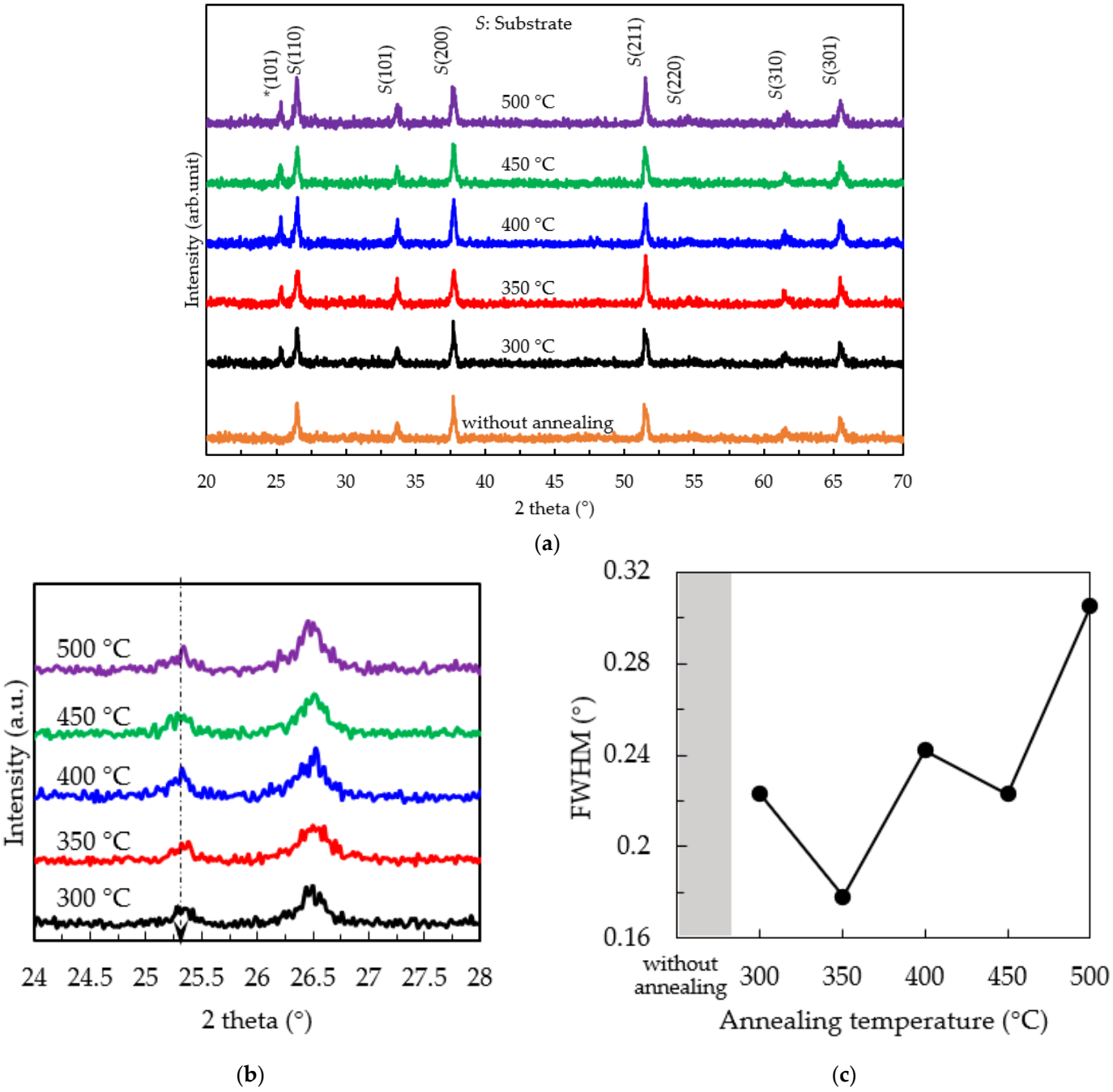

Figure 2. (**a**) The XRD patterns from 20° to 70° for the 7.5 wt%-injected TiO_2 film annealed at different temperatures from 300 to 500 °C; (**b**) the limited range of 24° to 28° for the undefined phase marked with a star, with (**c**) its variation in full width at the half maximum (FWHM) value.

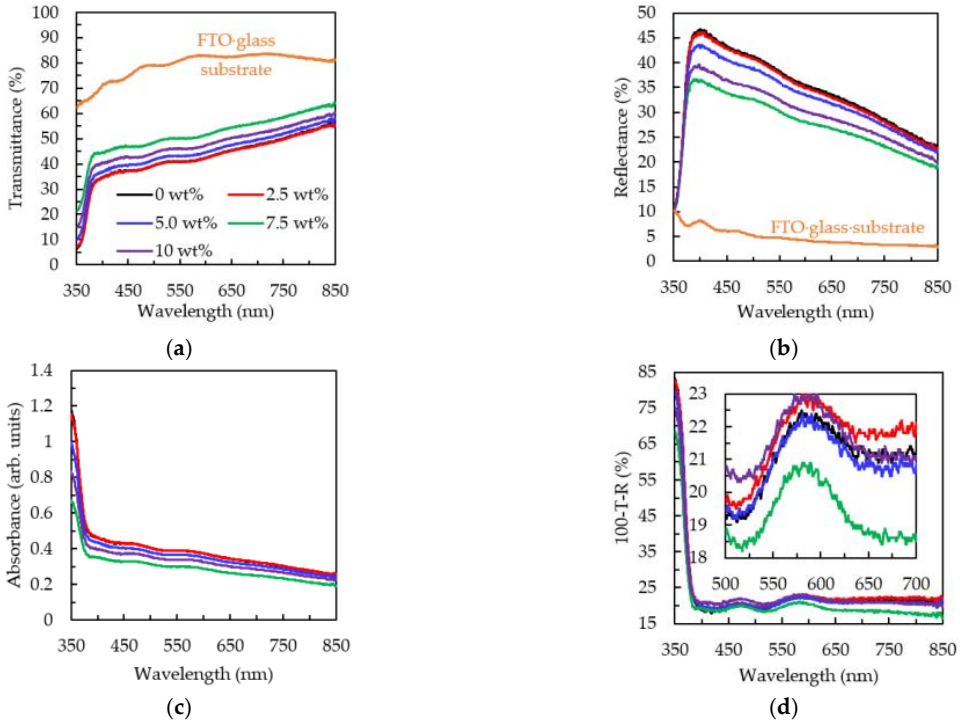

Figure 3. The (**a**) transmittance (T), (**b**) reflectance (R), (**c**) absorbance, and (**d**) haze spectra for the TiO_2 films prepared by injecting different DMF doses from 0 to 10 wt%, where the inserted haze image is in the range from 500 to 700 nm.

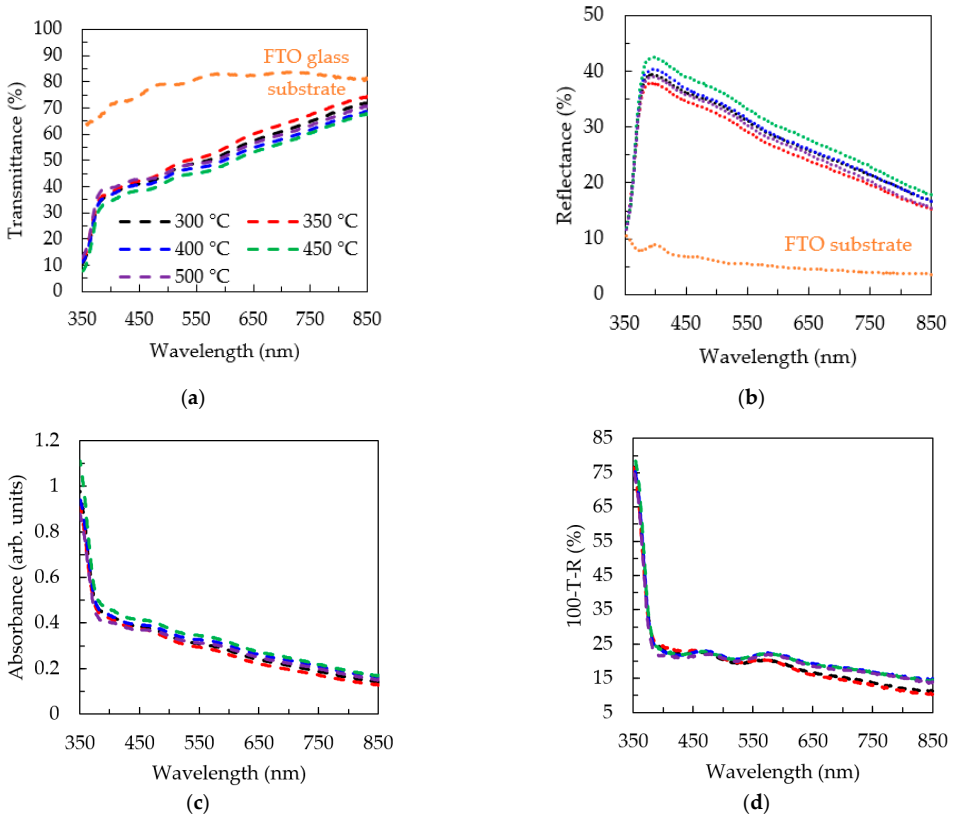

Figure 4. The (**a**) transmittance, (**b**) reflectance, (**c**) absorbance, and (**d**) the haze spectra for the 7.5 wt%-injected TiO_2 film annealed at different temperatures from 300 to 500 °C.

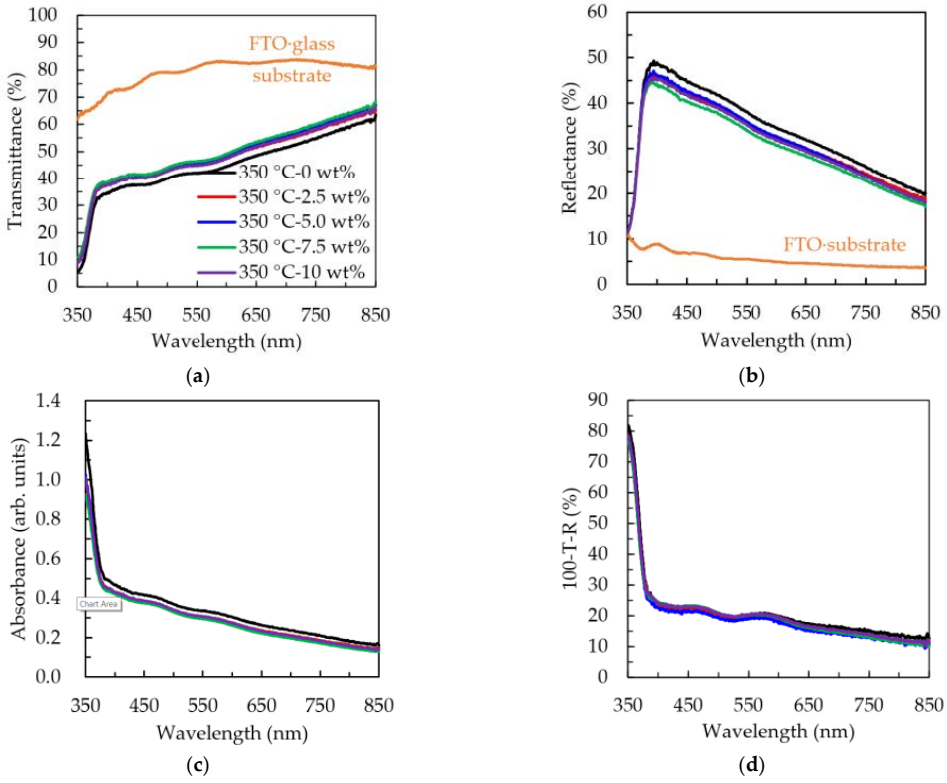

Figure 5. The (**a**) transmittance, (**b**) reflectance, (**c**) absorbance, and (**d**) haze spectra for the 350 °C-annealed TiO_2 film prepared by injecting different DMF doses from 0 to 10 wt%.

3.3. Effect of Comprehensive Comparison

In Figure 6, the Eg of the 7.5 wt%- injected TiO_2 film at 300 °C is 3.17 eV, and it reveals no change from 300 to 450 °C, and then slightly increases to 3.19 eV at 500 °C. The reason is that it is only when the annealing temperature is higher than 450 °C that sufficient forming energy is provided, resulting in the densest TiO_2 film. However, the Eg of the 350 °C-annealed TiO_2 film slightly decreases from 3.17 to 3.16 eV at the 2.5 wt% DMF dose and then increases to ~3.21 eV when increasing the DMF dose from 2.5 to 10 wt%. The slight Eg variation in TiO_2 film is affected by the DMF dose, revealing that the minor addition of DMF solvent obviously inhibits the aggregation of nanocrystalline structures and improves the film uniformity.

As shown in Figure 7, the topographic scanning electron microscope (SEM) images of 350 °C-annealed TiO_2 films prepared at different DMF doses from 0 to 10 wt% are observed. Each enlarged image is inserted to clearly estimate the crystallite size. With the increasing DMF doses, the film surface becomes denser due to the decreasing proportion of black cavities. Furthermore, the maximum long columnar shape observed and a clear increase in crystallite size to ~270 nm in Figure 7d indicate the densest 350 °C-annealed TiO_2 film. The excess 10 wt% DMF dose reveals the additional circular particle clusters. The estimated crystallite size distribution of the 350 °C-annealed TiO_2 films prepared by injecting different DMF doses from 0 to 10 wt% is approximate 169, 166, 174, 186, and 177 nm, respectively. It can be seen that the oxygen vacancies existing within the film defects act as the nucleation center to form the TiO_2 films due to the lower kinetics [47]. On the other hand, cross-cut testing was further used to demonstrate the film adhesion in Figure 8, revealing that better 350 °C-annealed TiO_2 films were prepared with 7.5 wt% DMF dose as compared to the other samples.

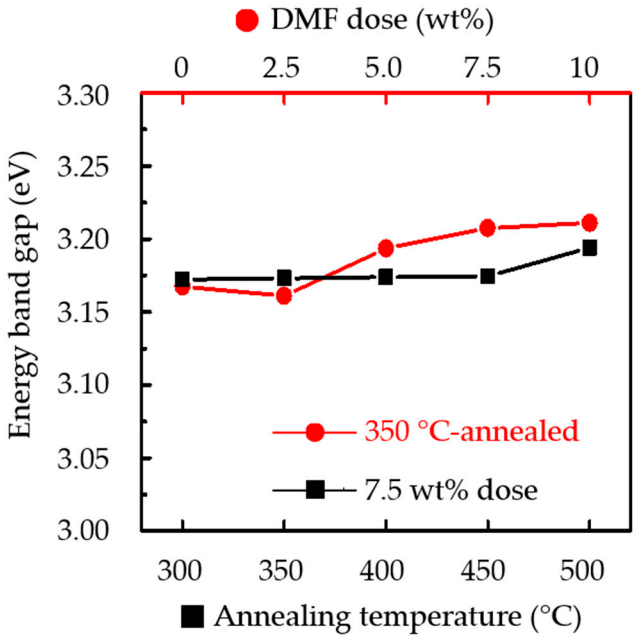

Figure 6. The variation of Eg for the 350 °C-annealed and 7.5 wt%-injected TiO_2 films prepared at various DMF doses and different annealing temperatures, respectively.

As shown in Figure 9, the porosity determined by the ImageJ software is defined by the ratio of the red area. The variation of determining porosity is shown in Figure 9f, illustrating that with the increasing DMF doses, the porosity value keeps consistent at ~40% from 0 to 5 wt%. The largest porosity of films is obtained at 350 °C, and then gradually decreases to 32.9% and 31.4% in the range of 7.5 to 10 wt%, respectively.

The cross-sectional and high-resolution transmission electron microscopy (TEM) images of 350 °C-annealed TiO_2 films prepared without and with 7.5 wt% DMF are shown in Figure 10a,b, respectively. The cross-sectional layers observed from top to bottom are identified as glue, TiO_2, FTO substrate, and SiO_2, respectively. The corresponding selected area electron diffraction images inserted into right side identify the single-crystal-like structure of the porous TiO_2 films. The obvious variation of distances between bright spots is observed, proving the existence of Ti_3O_5 phase-transition. The single-crystalline structure is demonstrated with the calculated d-spacing value as the high-resolution images in the image of the right side. Based on the energy-dispersive spectrometer result, the area of relative element distribution (O, Sn, Ti, and Si) presents that the black circuit shape from the TEM is the real TiO_2 particle, as shown in Figure 11. In Table 3, the carbon content of the 350 °C-annealed samples with and without the 7.5 wt% DMF dose are 10.26 and 8.94 at%, respectively. Meanwhile, the nitrogen content of all samples is 0%. Compared to the expected stoichiometry of TiO_2 film, the 350 °C-annealed samples with and without the 7.5 wt% DMF dose show O-to-Ti ($R_{O/Ti}$) atomic ratios of 1.85 and 2.23, respectively. This result shows that the increased 1.32 at% carbon content caused by the DMF solvent, which slightly increases the transmittance of ~7%, possibly since the carbon is an interstitial state of the TiO_2 crystal structure.

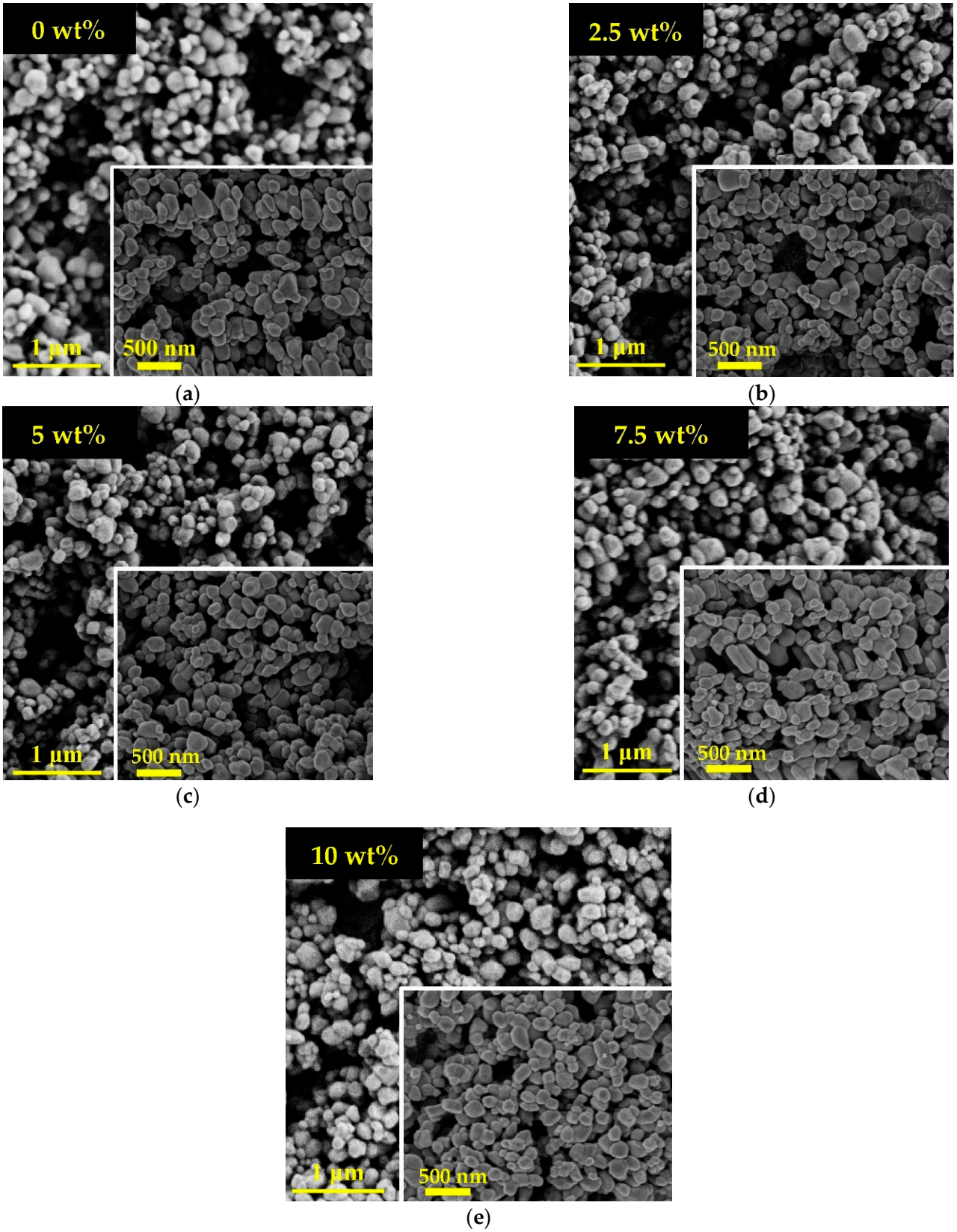

Figure 7. The cross-sectional SEM images of the 350 °C-annealed TiO_2 film prepared by injecting different DMF doses of (**a**) 0, (**b**) 2.5, (**c**) 5, (**d**) 7.5, and (**e**) 10 wt%.

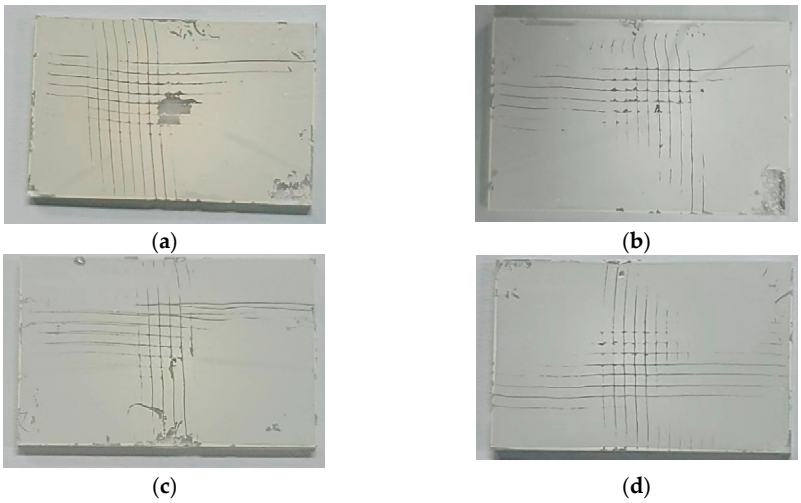

Figure 8. The cross-cut testing results of four samples, namely (**a**) without the annealing and DMF dose, (**b**) with 350 °C annealing, (**c**) with preparation of 7.5 wt% DMF dose, and (**d**) with the 350 °C annealing and 7.5 wt% DMF dose.

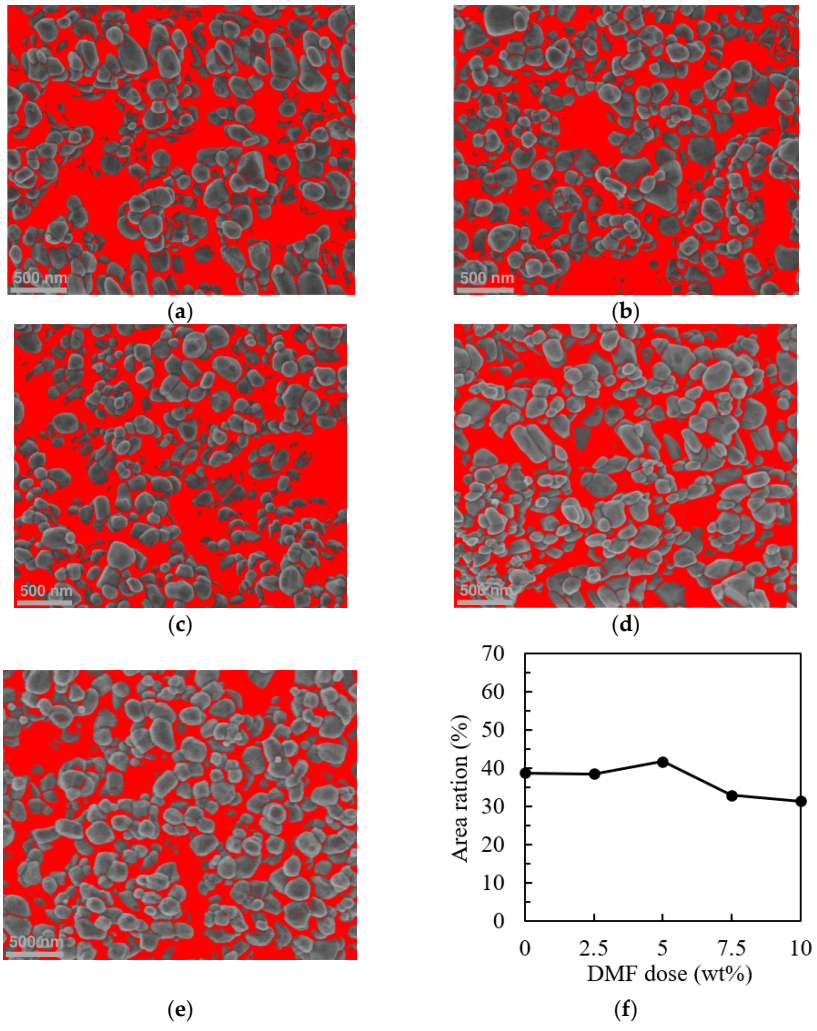

Figure 9. (**a**–**e**) The porosity characteristics of the samples prepared by injecting different DMF doses from 0 wt% to 10 wt%, and (**f**) the variation results.

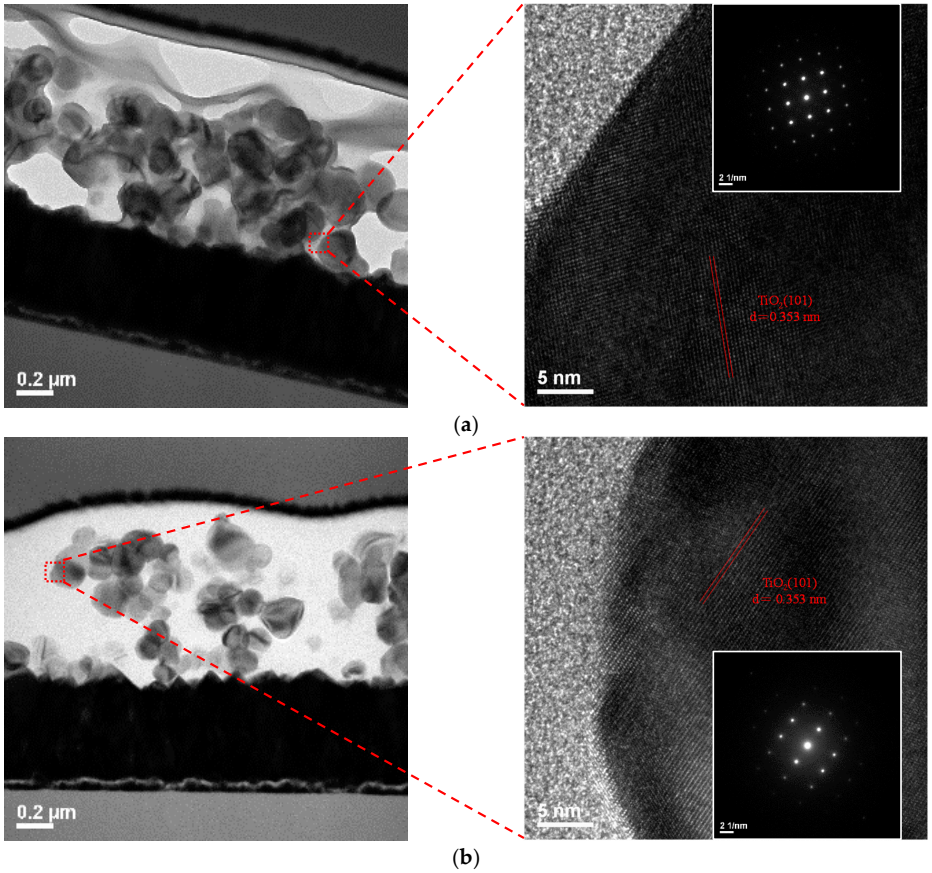

Figure 10. The cross-sectional and high-resolution TEM images for the 350 °C-annealed TiO_2 film prepared by injecting DMF doses of (**a**) 0 and (**b**) 7.5 wt%. The inserted image into the right side corresponds to the selected area electron diffraction images.

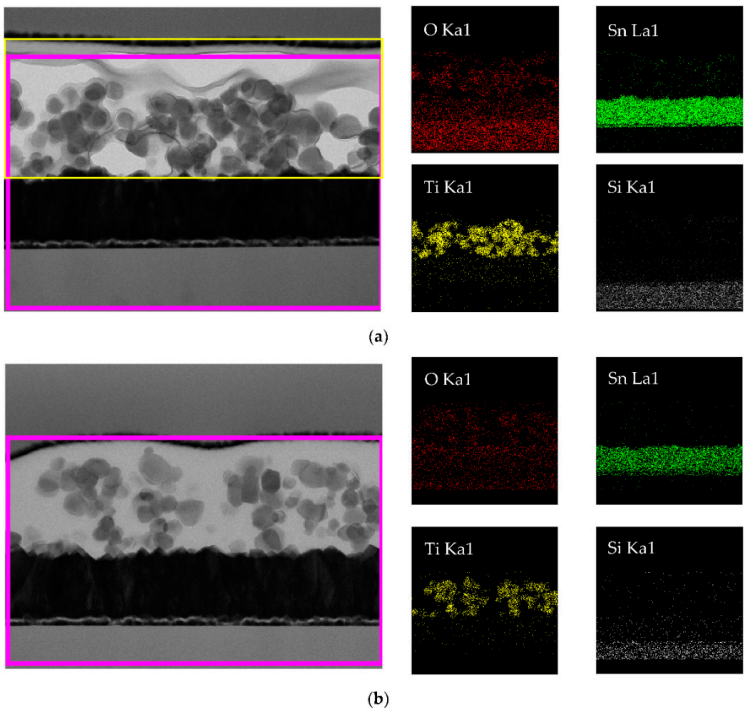

Figure 11. The energy-dispersive X-ray spectroscopy images of element distribution for the 350 °C-annealed TiO_2 film prepared (**a**) without and (**b**) with the 7.5 wt% DMF dose.

Table 3. The concentration of the carbon and nitrogen of the 350 °C-annealed samples with and without the 7.5 wt% DMF dose.

Sample		Carbon		Nitrogen		Oxygen		Titanium		O/Ti (Atomic Ratio)
DMF	Temp.	at%	wt%	at%	wt%	at%	wt%	at%	wt%	
without 7.5 wt%	350 °C	8.9	4.4	0	0	62.9	40.8	28.2	54.8	2.2
with 7.5 wt%	300 °C	10.2	4.7	0	0	57.7	35.7	32.2	59.6	1.8
	350 °C	10.3	4.8	0	0	58.2	36.3	31.5	58.9	1.9
	400 °C	9.5	4.4	0	0	58.6	36.4	31.9	59.2	1.8
	450 °C	10.5	5.3	0	0	63.2	42.1	26.3	52.6	2.4
	500 °C	7.6	3.4	0	0	57.6	34.4	34.8	62.2	1.7

However, as annealing temperatures rise, the $R_{O/Ti}$ ratios of 1.79, 1.85, and 1.84 at% in the range of 300–400 °C not only support the oxygen complement brought by air annealing, but also demonstrate that the lower temperatures of 300–400 °C provide the Ti and O atoms with sufficient diffusion activation energy to move to energetically favorable lattice sites. The film annealed at 450 °C has the highest $R_{O/Ti}$ of 2.4 at%, revealing the smaller grain size and the lowest transmittance. At 300–500 °C, on the other hand, the carbon content of samples is 10.15, 10.26, 9.45, 10.53, and the lowest is 7.6 at%, respectively. This result indicates that, in the range of 300–450 °C, the oxygen-insufficient TiO_2 film gradually becomes an oxygen-rich one via annealing. The removal of carbon caused by a higher annealing temperature from 450 to 500 °C reveals the oxygen-insufficient film with 1.66 at%, resulting in a decrease in carrier concentration due to the suppression of the formation energy of oxygen vacancies [48].

Consequently, in order to obtain the transparent conductive TiO_2 films, the electrical properties as a critical factor are worthy to be discussed. Figure 12 shows the carrier concentration (Ne), mobility (μ), and resistivity (ρ) determined by Hall effect measurements. In Figure 12a, the Ne of 2.55×10^{20} cm^{-3} slightly changes to 3.12×10^{20} cm^{-3} when the DMF dose is 2.5 wt%. Continuously, the highest Ne of 2.35×10^{21} cm^{-3} prepared with a 5.0 wt% DMF dose sharply decreases to ~3.15×10^{20} cm^{-3} at 7.5 and 10 wt% DMF. The μ of the film without the DMF dose is 51.67 $cm^2 \cdot V^{-1} \cdot s^{-1}$, and it dramatically reduces to the lowest 5.56 $cm^2 \cdot V^{-1} \cdot s^{-1}$ as injecting DMF dose to 5.0 wt%. The reason is attributed to the addition of the DMF solvent, causing the (110) phase formation of metastable crystalline near 25.28°, which is observed Ti_3O_5 (JCPDS card references: 23-0606); this is seen as a phase-transition based on the peak position shift. This shift toward a higher or lower angle leads to the lattice contraction or expansion, respectively. However, the 7.5 wt% DMF dose properly inhibits the proportion of coexisting crystalline phases. As shown in Figure 12b, the ρ of the films prepared by injecting different DMF doses is in the range of 4.74×10^{-4} and 4.85×10^{-4} ohm-cm, which is associated with the possible partial lattice mismatch in the TiO_2 films during crystallization, resulting in the optical loss at the long wavelength. Compared to the FTO film (4.46×10^{-4} ohm-cm) measured and other studies [45], this solvent-induced engineering can effectively tune the Ne and ρ of TiO_2 films. On the other hand, increasing the dripping DMF dose is able to prepare the highly transparent conductive TiO_2 film.

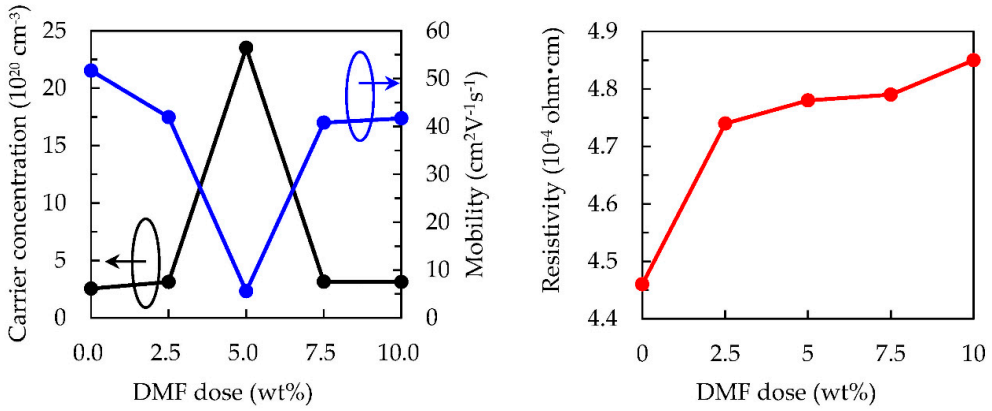

Figure 12. (**a**) Carrier concentration and mobility of the 350 °C-annealed TiO_2 film. (**b**) Resistivity determined by Hall effect measurement as a function of DMF doses from 0 to 10 wt%.

4. Conclusions

The porous TiO_2 films with a single-crystal-like structure are prepared by injecting DMF doses from 0 to 10 wt%. These solvent-induced TiO_2 films are also annealed at different temperatures from 300 to 500 °C. For the optoelectronic devices, such as solar cells, optical sensors, and biomedicine engineering, the porous TiO_2 film needs high transmittance or low reflectance to increase the light utilization efficiency. With the increase in DMF injection, the 7.5 wt% DMF indicates the best optical properties of transmittance and reflectance. However, the porous TiO_2 films prepared by 5 wt% DMF demonstrates the optimized carrier concentration of 2.35×10^{21} cm^{-3} after the low-annealing temperature of 350 °C. The production of carbon and oxygen atoms of the carbonyl group (CO) bonds and the carbon-containing compounds during volatilization may exist in the crystal structure with the defect or interstitial state. Compared to the samples with and without annealing, the appearance of the unique (101) peak near 25.2° proves the single-crystalline structure of porous TiO_2 films, and the slight shift of peak position proves the lattice expansion and contraction at lower and higher than 350 °C, respectively. The sample at 350 °C also shows the lowest FWHM value, suggesting the phase-transition phenomena between β-TiO_2 and λ-TiO_2. Another possible reason can be attributed to the fact that the non-stoichiometric components of Ti metal are induced by the addition of DMF solvent bonds with the oxygen.

Author Contributions: Conceptualization, P.-H.H. and C.-J.H.; methodology, P.-H.H., C.-H.W. and C.-K.W.; validation, Y.-Q.Z. and J.L.; formal analysis, P.-H.H., Y.-Q.Z. and C.-J.H.; investigation, P.-H.H., C.-H.W. and C.-K.W.; resources, J.L. and C.-J.H.; data curation, C.-H.W., C.-K.W. and Y.-Q.Z.; writing—original draft preparation, P.-H.H.; writing—review and editing, K.-W.L. and C.-J.H.; visualization, P.-H.H., C.-H.W., C.-K.W. and Y.-Q.Z.; supervision, K.-W.L. and C.-J.H.; project administration, P.-H.H., K.-W.L. and C.-J.H.; funding acquisition, C.-J.H. All authors have read and agreed to the published version of the manuscript.

Funding: This research was funded by the National Science and Technology Council (NSTC) of Taiwan under the following contract numbers: NSTC 109-2221-E-390-008 and NSTC 110-2221-E-390-019.

Acknowledgments: We appreciate the effort from Hsiu-Ling Huang and the Micro & Nano Semiconductor Research Center of Jimei University for the administrative and technical support.

Conflicts of Interest: The authors declare no conflict of interest.

References

1. Lee, K.; Jung, S.; Son, H.; Jang, K.; Lee, J.; Park, H.; Kim, J.; Kim, K.; Yi, J. Application of a Gate Blocking Layer on Glass by Using TiO_2 as a High-k Material for a Nonvolatile Memory. *J. Korean Phys. Soc.* **2008**, *52*, 1863–1867. [CrossRef]
2. Liu, J.W.; Liao, M.Y.; Imura, M.; Banal, R.G.; Koide, Y. Deposition of TiO_2 / Al_2O_3 Bilayer on Hydrogenated Diamond for Electronic Devices: Capacitors, Field-Effect Transistors, and Logic Inverters. *J. Appl. Phys.* **2017**, *121*, 224502. [CrossRef]

3. Hu, C.; McDaniel, M.D.; Posadas, A.; Demkov, A.A.; Ekerdt, J.G.; Yu, E.T. Highly Controllable and Stable Quantized Conductance and Resistive Switching Mechanism in Single-Crystal TiO_2 Resistive Memory on Silicon. *Nano Lett.* **2014**, *14*, 4360–4367. [CrossRef]
4. Geiger, M.; Lingstädt, R.; Wollandt, T.; Deuschle, J.; Zschieschang, U.; Letzkus, F.; Burghartz, J.N.; Aken, P.A.; Weitz, R.T.; Klauk, H. Subthreshold Swing of 59 MV Decade^{-1} in Nanoscale Flexible Ultralow-Voltage Organic Transistors. *Adv. Electron. Mater.* **2022**, *8*, 2101215. [CrossRef]
5. Chu, Y.-M.; Lin, C.-C.; Chang, H.-C.; Li, C.; Guo, C. TiO_2 Nanowire FET Device: Encapsulation of Biomolecules by Electro Polymerized Pyrrole Propylic Acid. *Biosens. Bioelectron.* **2011**, *26*, 2334–2340. [CrossRef]
6. Lo, S.-Y.; Wuu, D.-S.; Chang, C.-H.; Wang, C.-C.; Lien, S.-Y.; Horng, R.-H. Fabrication of Flexible Amorphous-Si Thin-Film Solar Cells on a Parylene Template Using a Direct Separation Process. *IEEE Trans. Electron Devices* **2011**, *58*, 1433–1439. [CrossRef]
7. Yang, C.-H.; Lien, S.-Y.; Chu, C.-H.; Kung, C.-Y.; Cheng, T.-F.; Chen, P.-T. Effectively Improved SiO_2-TiO_2 Composite Films Applied in Commercial Multicrystalline Silicon Solar Cells. *Int. J. Photoenergy* **2013**, *2013*, 823254. [CrossRef]
8. Lin, Y.-S.; Lien, S.-Y.; Wuu, D.-S.; Huang, Y.-X.; Kung, C.-Y. Improvement in Performance of Si-Based Thin Film Solar Cells with a Nanocrystalline SiO_2-TiO_2 Layer. *Thin Solid Films* **2014**, *570*, 200–203. [CrossRef]
9. Hsu, C.-H.; Chen, K.-T.; Huang, P.-H.; Wu, W.-Y.; Zhang, X.-Y.; Wang, C.; Liang, L.-S.; Gao, P.; Qiu, Y.; Lien, S.-Y.; et al. Effect of Annealing Temperature on Spatial Atomic Layer Deposited Titanium Oxide and Its Application in Perovskite Solar Cells. *Nanomaterials* **2020**, *10*, 1322. [CrossRef]
10. Huang, P.-H.; Huang, C.-W.; Kang, C.-C.; Hsu, C.-H.; Lien, S.-Y.; Wang, N.-F.; Huang, C.-J. The Investigation for Coating Method of Titanium Dioxide Layer in Perovskite Solar Cells. *Crystals* **2020**, *10*, 236. [CrossRef]
11. Hsu, C.-H.; Chen, K.-T.; Liang, L.-S.; Gao, P.; Ou, S.-L.; Wu, W.-Y.; Huang, P.-H.; Lien, S.-Y. Improved Perovskite Solar Cell Performance by High Growth Rate Spatial Atomic Layer Deposited Titanium Oxide Compact Layer. *IEEE J. Electron Devices Soc.* **2021**, *9*, 49–56. [CrossRef]
12. Latif, H.; Azher, Z.; Shabbir, S.A.; Rasheed, S.; Pervaiz, E.; Sattar, A.; Imtiaz, A. A Novel Leaves and Needles like TiO_2 (LNT) Electron Transfer Layer (ETL) as an Alternative to Meso-Porous TiO_2 Electron Transfer Layer (ETL) in Perovskite Solar Cell. *Opt. Mater.* **2020**, *109*, 110281. [CrossRef]
13. Murugadoss, G.; Mizuta, G.; Tanaka, S.; Nishino, H.; Umeyama, T.; Imahori, H.; Ito, S. Double Functions of Porous TiO_2 Electrodes on $CH_3NH_3PbI_3$ Perovskite Solar Cells: Enhancement of Perovskite Crystal Transformation and Prohibition of Short Circuiting. *APL Mater.* **2014**, *2*, 081511. [CrossRef]
14. Karunagaran, B.; Uthirakumar, P.; Chung, S.J.; Velumani, S.; Suh, E.-K. TiO_2 Thin Film Gas Sensor for Monitoring Ammonia. *Mater. Charact.* **2007**, *58*, 680–684. [CrossRef]
15. Ramanavicius, S.; Tereshchenko, A.; Karpicz, R.; Ratautaite, V.; Bubniene, U.; Maneikis, A.; Jagminas, A.; Ramanavicius, A. TiO_2-x/TiO_2-Structure Based 'Self-Heated' Sensor for the Determination of Some Reducing Gases. *Sensors* **2019**, *20*, 74. [CrossRef]
16. Chen, J.-Z.; Ko, W.-Y.; Yen, Y.-C.; Chen, P.-H.; Lin, K.-J. Hydrothermally Processed TiO_2 Nanowire Electrodes with Antireflective and Electrochromic Properties. *ACS Nano* **2012**, *6*, 6633–6639. [CrossRef]
17. Choi, Y.; Kim, K.-W.; In, Y.R.; Tang, X.; Kim, P.; Quy, V.H.V.; Kim, Y.M.; Lee, J.; Choi, C.; Jung, C.; et al. Multicolor, Dual-Image, Printed Electrochromic Displays Based on Tandem Configuration. *Chem. Eng. J.* **2022**, *429*, 132319. [CrossRef]
18. Fujishima, A.; Honda, K. Electrochemical Photolysis of Water at a Semiconductor Electrode. *Nature* **1972**, *238*, 37–38. [CrossRef]
19. Li, D.; Bulou, S.; Gautier, N.; Elisabeth, S.; Goullet, A.; Richard-Plouet, M.; Choquet, P.; Granier, A. Nanostructure and Photocatalytic Properties of TiO_2 Films Deposited at Low Temperature by Pulsed PECVD. *Appl. Surf. Sci.* **2019**, *466*, 63–69. [CrossRef]
20. Lee, H.Y.; Park, Y.H.; Ko, K.H. Correlation between Surface Morphology and Hydrophilic/Hydrophobic Conversion of MOCVD-TiO_2 Films. *Langmuir* **2000**, *16*, 7289–7293. [CrossRef]
21. Justh, N.; Mikula, G.J.; Bakos, L.P.; Nagy, B.; László, K.; Parditka, B.; Erdélyi, Z.; Takáts, V.; Mizsei, J.; Szilágyi, I.M. Photocatalytic Properties of TiO_2@polymer and TiO_2@carbon Aerogel Composites Prepared by Atomic Layer Deposition. *Carbon* **2019**, *147*, 476–482. [CrossRef]
22. Bokov, D.; Turki Jalil, A.; Chupradit, S.; Suksatan, W.; Javed Ansari, M.; Shewael, I.H.; Valiev, G.H.; Kianfar, E. Nanomaterial by Sol-Gel Method: Synthesis and Application. *Adv. Mater. Sci. Eng.* **2021**, *2021*, 5102014. [CrossRef]
23. Wang, H.-E.; Jin, J.; Cai, Y.; Xu, J.-M.; Chen, D.-S.; Zheng, X.-F.; Deng, Z.; Li, Y.; Bello, I.; Su, B.-L. Facile and Fast Synthesis of Porous TiO_2 Spheres for Use in Lithium Ion Batteries. *J. Colloid Interface Sci.* **2014**, *417*, 144–151. [CrossRef] [PubMed]
24. da Silva, A.L.; Trindade, F.J.; Dalmasso, J.-L.; Ramos, B.; Teixeira, A.C.S.C.; Gouvêa, D. Synthesis of TiO_2 Microspheres by Ultrasonic Spray Pyrolysis and Photocatalytic Activity Evaluation. *Ceram. Int.* **2022**, *48*, 9739–9745. [CrossRef]
25. Noman, M.T.; Ashraf, M.A.; Ali, A. Synthesis and Applications of Nano-TiO_2: A Review. *Environ. Sci. Pollut. Res.* **2019**, *26*, 3262–3291. [CrossRef] [PubMed]
26. Cao, F.; Xiong, J.; Wu, F.; Liu, Q.; Shi, Z.; Yu, Y.; Wang, X.; Li, L. Enhanced Photoelectrochemical Performance from Rationally Designed Anatase/Rutile TiO_2 Heterostructures. *ACS Appl. Mater. Interfaces* **2016**, *8*, 12239–12245. [CrossRef]
27. Lupu, A. Combined In Vitro Effects of TiO_2 Nanoparticles and Dimethyl Sulfoxide (DMSO) on HepG2 Hepatocytes. *Int. J. Nanomater. Nanotechnol. Nanomed.* **2015**, *1*, 002–010. [CrossRef]
28. You, M.S.; Heo, J.H.; Park, J.K.; Moon, S.H.; Park, B.J.; Im, S.H. Low Temperature Solution Processable TiO_2 Nano-Sol for Electron Transporting Layer of Flexible Perovskite Solar Cells. *Sol. Energy Mater. Sol. Cells* **2019**, *194*, 1–6. [CrossRef]

29. Guai, G.H.; Song, Q.L.; Lu, Z.S.; Ng, C.M.; Li, C.M. Tailor and Functionalize TiO_2 Compact Layer by Acid Treatment for High Performance Dye-Sensitized Solar Cell and Its Enhancement Mechanism. *Renew. Energy* **2013**, *51*, 29–35. [CrossRef]
30. Sarraf, M.; Nasiri-Tabrizi, B.; Yeong, C.H.; Madaah Hosseini, H.R.; Saber-Samandari, S.; Basirun, W.J.; Tsuzuki, T. Mixed Oxide Nanotubes in Nanomedicine: A Dead-End or a Bridge to the Future? *Ceram. Int.* **2021**, *47*, 2917–2948. [CrossRef]
31. Sun, W.; Liu, H.; Hu, J.; Li, J. Controllable Synthesis and Morphology-Dependent Photocatalytic Performance of Anatase TiO_2 Nanoplates. *RSC Adv.* **2015**, *5*, 513–520. [CrossRef]
32. Yao, M.; Ji, Y.; Wang, H.; Ao, Z.; Li, G.; An, T. Adsorption Mechanisms of Typical Carbonyl-Containing Volatile Organic Compounds on Anatase TiO_2 (001) Surface: A DFT Investigation. *J. Phys. Chem. C* **2017**, *121*, 13717–13722. [CrossRef]
33. Feng, X.; Li, Z. Photocatalytic Promoting Dimethylformamide (DMF) Decomposition to in-Situ Generation of Self-Supplied CO for Carbonylative Suzuki Reaction. *J. Photochem. Photobiol. A Chem.* **2017**, *337*, 19–24. [CrossRef]
34. Ma, T.; Tadaki, D.; Sakuraba, M.; Sato, S.; Hirano-Iwata, A.; Niwano, M. Effects of Interfacial Chemical States on the Performance of Perovskite Solar Cells. *J. Mater. Chem. A* **2016**, *4*, 4392–4397. [CrossRef]
35. de Oliveira, C.V.; Migot, S.; Alhussein, A.; Jiménez, C.; Schuster, F.; Ghanbaja, J.; Sanchette, F. Structural and Microstructural Analysis of Bifunctional TiO_2/Al-Zr Thin Film Deposited by Hybrid Process. *Thin Solid Films* **2020**, *709*, 138255. [CrossRef]
36. Ghazaryan, L.; Handa, S.; Schmitt, P.; Beladiya, V.; Roddatis, V.; Tünnermann, A.; Szeghalmi, A. Structural, Optical, and Mechanical Properties of TiO_2 Nanolaminates. *Nanotechnology* **2021**, *32*, 095709. [CrossRef]
37. Ohkoshi, S.; Tsunobuchi, Y.; Matsuda, T.; Hashimoto, K.; Namai, A.; Hakoe, F.; Tokoro, H. Synthesis of a Metal Oxide with a Room-Temperature Photoreversible Phase Transition. *Nat. Chem.* **2010**, *2*, 539–545. [CrossRef]
38. Anuchai, S.; Phanichphant, S.; Tantraviwat, D.; Pluengphon, P.; Bovornratanaraks, T.; Inceesungvorn, B. Low Temperature Preparation of Oxygen-Deficient Tin Dioxide Nanocrystals and a Role of Oxygen Vacancy in Photocatalytic Activity Improvement. *J. Colloid Interface Sci.* **2018**, *512*, 105–114. [CrossRef]
39. Kassiba, A.; Pattier, B.; Henderson, M.; Makowska-Janusik, M.; Mei, P.; Gibaud, A. Titanium Oxide Based Mesoporous Powders and Gels: Doping Effects and Photogenerated Charge Transfer. *Mater. Sci. Eng. B-Adv. Funct. Solid-State Mater.* **2012**, *177*, 1446–1451. [CrossRef]
40. Tański, T.; Matysiak, W. Synthesis of the Novel Type of Bimodal Ceramic Nanowires from Polymer and Composite Fibrous Mats. *Nanomaterials* **2018**, *8*, 179. [CrossRef]
41. de Farias, F.R.; Silva, C.C.G.; Restivo, T.A.G. Thermal Study of the Anatase-Rutile Structural Transitions in Sol-Gel Synthesized Titanium Dioxide Powders. *J. Serb. Chem. Soc.* **2005**, *70*, 675–679. [CrossRef]
42. Santara, B.; Giri, P.K.; Imakita, K.; Fujii, M. Microscopic Origin of Lattice Contraction and Expansion in Undoped Rutile TiO_2 Nanostructures. *J. Phys. D Appl. Phys.* **2014**, *47*, 215302. [CrossRef]
43. Jacob, M.M.E.; Arof, A.K. FTIR Studies of DMF Plasticized Polyvinyledene Fluoride Based Polymer Electrolytes. *Electrochim. Acta* **2000**, *45*, 1701–1706. [CrossRef]
44. Mechiakh, R.; Sedrine, N.B.; Chtourou, R.; Bensaha, R. Correlation between Microstructure and Optical Properties of Nano-Crystalline TiO_2 Thin Films Prepared by Sol-Gel Dip Coating. *Appl. Surf. Sci.* **2010**, *257*, 670–676. [CrossRef]
45. Gomez-Hermoso-de-Mendoza, J.; Gutierrez, J.; Tercjak, A. Improvement of Macroscale Properties of TiO_2/Cellulose Acetate Hybrid Films by Solvent Vapour Annealing. *Carbohydr. Polym.* **2020**, *231*, 115683. [CrossRef]
46. Estruga, M.; Domingo, C.; Domènech, X.; Ayllón, J.A. Low Temperature *N*, *N*-Dimethylformamide-Assisted Synthesis and Characterization of Anatase-Rutile Biphasic Nanostructured Titania. *Nanotechnology* **2009**, *20*, 125604. [CrossRef]
47. Luka, G.; Witkowski, B.S.; Wachnicki, L.; Andrzejczuk, M.; Lewandowska, M.; Godlewski, M. Kinetics of Anatase Phase Formation in TiO_2 Films during Atomic Layer Deposition and Post-Deposition Annealing. *Crystengcomm* **2013**, *15*, 9949. [CrossRef]
48. Pan, X.; Yang, M.-Q.; Fu, X.; Zhang, N.; Xu, Y.-J. Defective TiO_2 with Oxygen Vacancies: Synthesis, Properties and Photocatalytic Applications. *Nanoscale* **2013**, *5*, 3601. [CrossRef]